Laser surface texturing of a WC-CoNi cemented carbide grade: Surface topography design for honing application

Shiqi Fang[1,2,3], Luis Llanes[1,2], Dirk Bähre[3]

[1]CIEFMA-Departament de Ciència del Materials i Enginyeria Metal.lúrgica, Universitat Politècnica de Catalunya, EEBE - Campus Diagonal Besòs, 08019 Barcelona, Spain

[2]Barcelona Research Center in Multiscale Science and Engineering, Universitat Politècnica de Catalunya, 08019 Barcelona

[3]Institute of Production Engineering, Saarland University, 66123 Saarbrücken, Germany

* corresponding author:

Prof. Luis Llanes

EEBE-Universitat Politècnica de Catalunya
C/ Eduard Maristany, 10-14
08019 Barcelona Spain
luis.miguel.llanes@upc.edu

Abstract. Abrasive effectiveness of composite-like honing stones is related to the intrinsic surface topography resulting from the cubic boron nitride (CBN) grains protruding out of the metallic matrix. Within this framework, Laser Surface Texturing (LST) is implemented for replicating topographic features of a honing stone in a WC-base cemented carbide grade, commonly employed for making tools. In doing so, regular arrays of hexagonal pyramids (similar to CBN grains) are sculpted by a laser micromachining system. Micrometric precision is attained and surface integrity does not get affected by such surface modification. Finally, potential of laser-patterned cemented carbide tools, as alternative to conventional honing stones, is supported by successful material removal and enhanced surface smoothness of a steel workpiece in the abrasive testing.

Keywords: Surface Modification; Cemented Carbide; Abrasive Processes; Surface Integrity

1. Introduction

Honing stones employed for precision machining applications are usually fabricated from composites consisting of cubic boron nitride particles, acting as super hard abrasives, embedded in a metallic matrix. In general, the abrasive effectiveness of honing stones is directly related to the intrinsic surface topography resulting from the super hard grains protruding out of the matrix (e.g. Ref. [1]). In this regard, the use of more conventional hard materials may be proposed for this tooling application, as far as the surface topography features of current honing stones could be replied at the corresponding length scales. Considering that cemented carbides may be an interesting option, potential success of this approach will widen out the range of properties of honing tools, as a direct function of the quite variable range of microstructural assemblages existing for these materials [2]. Surface texturing of structural materials usually yields improved functional performance, significant life extension and even wider application opportunities [3,4]. Within this context, special attention has been paid to tribological application of textured surfaces, particularly aiming for reduction of friction between contact surfaces [5-7]. For instance, geometrical properties of grooves have been found to exhibit a strong impact on the lubricant distribution of piston rings [8].

Laser surface texturing (LST) using ultra-short pulse laser has become a popular micromachining method [9,10]. It is particularly suitable for tiny parts with high precision and short time machining requirements. During LST processing, the ultra-short pulse laser has extreme short reaction time with the target material. Thus, material is removed by cold ablation rather than by thermal reaction, i.e. melting and vaporization. As a result, thermal damage may be effectively diminished. This highlights a noticeable advantage of LST over other non-abrasive surface texturing options, e.g. electrical discharge machining (EDM), regarding surface patterning of cemented carbides [11,12].

Potential of LST as surface modification technology, especially in cemented carbides, has been reported in literature [13-17]. However, investigation about this subject is rather scarce, and mainly focused on the influence of basic LST patterning or shaping on tribological performance. In this regard, implementation of LST has shown to be beneficial for both grinding tools, as cutting edges are readily exposed, and turning ones, as supplementary tool-chip interface is created [18,19]. Furthermore, capability of laser machining to shape cutting edge roundness of cemented carbides has been recently demonstrated [20]. More complex patterns, as those associated with surface topography of honing tools, require precise movement control of laser beams. In a recent study, the authors have proven the capability of high precision 5-axis laser micromachining system, combined with a picosecond laser, to move the beams along the x-, y- and z- axis with micrometric precision [21].

Such accurate movement of laser beams, especially their oscillation in the perpendicular direction to the workpiece, facilitates the production of complex surface structures. Such technical development can not only widen the application range of LST but also open windows for creative surface topography design. An example of successful application of this approach is found on enhanced abrasive ability and/or lubrication efficiency of grinding wheels by means of manufactured surface topography, in terms of either micro-texturing or defined ceramic grain patterns [22-24].

In this study, LST is employed to reproduce the surface topography of a conventional honing stone on the surface of a WC-CoNi cemented carbide grade. It was programmed to induce simultaneous movement along the x-, y-, z- axis of the laser beams, such to remove very tiny volumes of the cemented carbide (workpiece) and sculpt grain-like pyramids from the surface. Once aimed surface topography was shaped, geometrical features of LST surface were measured and resulting surface integrity was assessed. Finally, performance of a cemented carbide tool with the LST textured surface was tested in a workbench designed to simulate an external honing (cutting) process.

2. Novel cemented carbide tool conception

2.1. Fundamental ideas

Although CBN composites and cemented carbides are commonly employed for fabricating cutting tools, their effective implementation depends on cutting conditions and requirements. CBN composites are more appropriated for non-conventional abrasive machining processes, such as grinding and honing. Here, workpiece material is removed by a multitude of tiny cutting edges formed by the protruding grains, with size ranging from 2 to 250 µm (**Figure 1(a)**) [25]. On the other hand, cemented carbides are usually employed in chip-removal machining processes, such as turning and milling. Under these conditions, workpiece material is removed rather by one cutting edge in connection with different feeding movements. The cutting edge is then composed of several (many) carbide grains, with size ranging from 0.5 to 30 µm, and should be shaped prior to the application as cutting tool (**Figure 1(b)**).

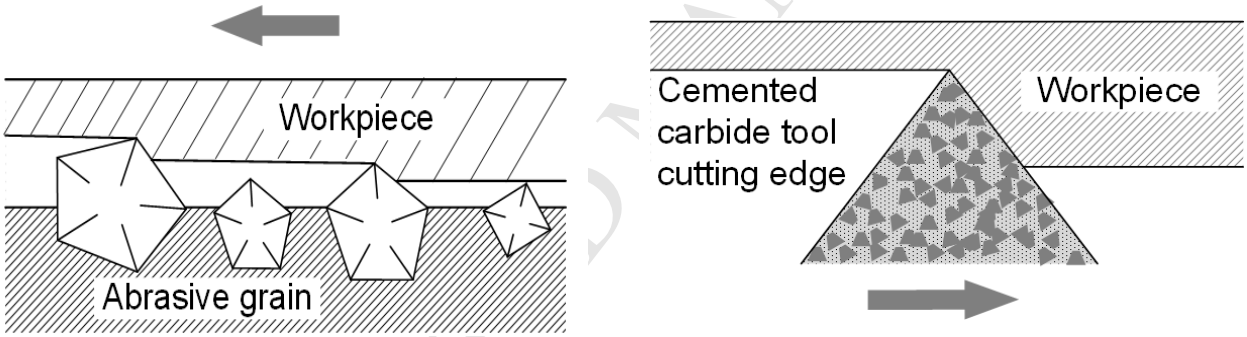

(a) (b)

Figure 1. Schematic illustration of material removal in (a) abrasive machining processes (where CBN composite is used as cutting tool); (b) chip-removal machining processes (where cemented carbide is used as cutting tool).

A critical step of this study was to replicate the surface topography of reference honing tool (associated with exposed abrasive grains) on the cemented carbide surface by means of LST. This effectively means shaping tiny cutting edges at the cemented carbide surfaces **(Figure 2(a))**. Considering that size difference of abrasive particles for conventional honing tools and the studied cemented carbide grade may be as large as 10 times **(Figure 2(b))**, the implemented approach here was to sculpture pyramids (similar to CBN grains) out of the cemented carbide's surface by means of high precision LST. The formed cutting edges should possess similar geometrical features as CBN grains, aiming to endow a surface topography with similar cutting ability as the one exhibited by CBN composites **(Figure 2(c))**.

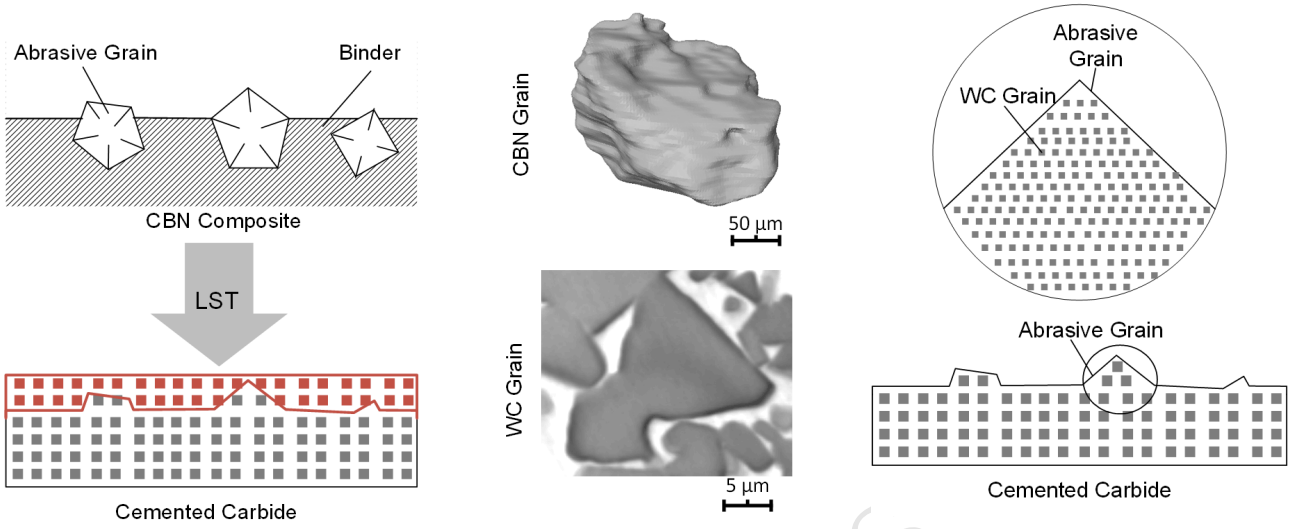

(a) (b)

Figure 2. (a) Schematic illustration of novel tool fabrication concept for honing processes; (b) grain size comparison between CBN grain and WC grain of the studied materials; (c) fabrication of abrasive grain with WC grains.

2.2. Design of geometrical features for surface topography of the new tool

In a recent work, authors have provided a detailed quantitative characterization of surface topography of a conventional honing stone, tagged as B151, which will be used here as reference condition [26]. It was done following an experimental protocol consisting of five steps: specimen preparation, surface scanning, image assembly, image digital processing and final surface quantification. It also involved the use of laser scanning microscopy (LSM) and digital imaging processing for assessing significant dimensional, geometrical and positional properties of CBN grains at the surface of B151 honing stone. Measured properties are listed in **Table 1.** Taking into account the microstructural assemblage of the reference honing tool, aimed surface topography for being laser-induced on the WC-CoNi cemented carbide was defined to consist of patterns of sculpted hexagonal pyramids with similar microstructural properties. Surface topography features aimed for the WC-CoNi cemented carbide are also included in **Table 1**. The pyramids were designed to be located in array distribution with identical interval. Although it does not match the irregular grain location on the surface of B151, this was not aimed because it is believed that regular distribution and grain shape can improve the tool performance [22,27,28]. Furthermore, regular arrays facilitate measurement of geometrical features and evaluation of LST machining influence. For each single pyramid, the following parameters were used to describe the geometrical features (**Figure 3**):

d_1 : interval between two adjacent hexagonal pyramid along the x-axis

d_2 : interval between two adjacent hexagonal pyramid along the y-axis

a_1 : bottom side length of the hexagonal pyramid

a_2 : top side length of the hexagonal pyramid

S_1 : surface area of the pyramid bottom

S_2 : surface area of the pyramid top

h : height the hexagonal pyramid

α: slope at the measuring position A-A

β: slope at the measuring position B-B

Table 1. Microstructural properties of the honing stone B151 and aimed surface topography features for the WC-CoNi cemented carbide sample

Sample	Grain quantity	Sample surface ($x10^7$ µm²)	Total grain surface area ($x10^6$ µm²)	Phase ratio	Grain shape
B151	355	4.2	3.8	8.9%	Most varying from rectangle to hexagon
WC-CoNi	343	6	5	8.3%	Hexagon

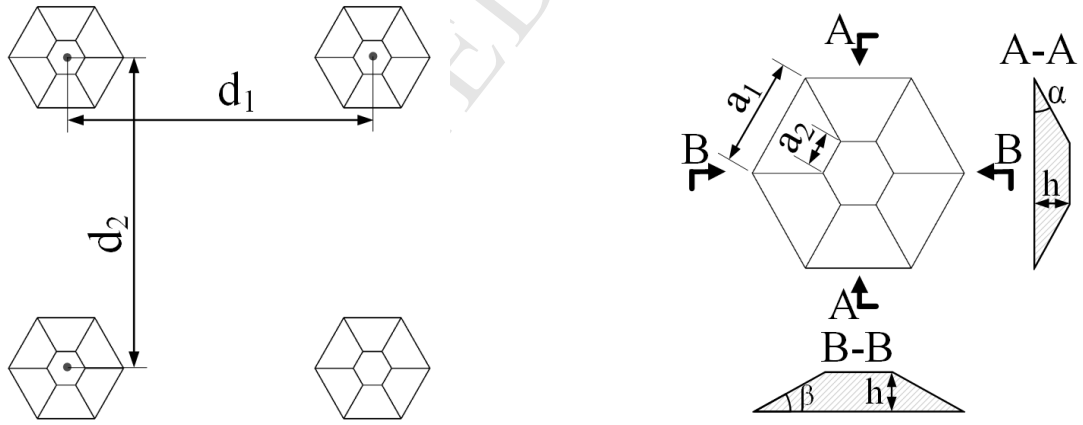

(a) (b)

Figure 3. Geometrical parameters involved in the surface topography design aimed to simulate microstructural assemblage of B151 honing tool: (a) pyramid distribution, (b) geometry of single hexagonal pyramid.

Hence, surface patterning action was aimed to sculpt hexagonal pyramids regularly distributed along the x- and y- axis, separated from each other, d_1 and d_2 respectively, about 400 µm in both directions. Furthermore, side lengths a_1 and a_2 were defined as 75 µm and 25 µm respectively, with a height h

of 25 µm. Under this geometrical consideration, surface areas S_1 and S_2, at the pyramid bottom and top respectively, resulted to be 14.6×10³ µm² and 1.6×10³ µm². Moreover, inclination angles between the bottom and the top of the pyramid were aimed to achieve slopes α (at the measuring position A-A) and β (at the measuring position B-B) of 30.0° and 26.6º respectively. All these parameters are listed in **Table 2**.

Table 2. Geometrical parameters aimed for LST hexagonal pyramid patterns.

Parameters	d_1 (µm)	d_2 (µm)	a_1 (µm)	a_2 (µm)	S_1 (µm²)	S_2 (µm²)	h (µm)	α (°)	β (°)
Design	400	400	75	25	14.6×10^3	1.6×10^3	25	30.0	26.6

$S = \frac{3}{2}\sqrt{3}a^2, a_1 = 75\mu m, a_2 = 25\mu m$

3. Experimental aspects

3.1 Studied materials

A WC-CoNi cemented carbide grade (commonly referred to as hardmetal because its WC-base nature) was investigated (**Figure 4(a)**). It consisted of WC grains embedded in a 28 wt% metallic (CoNi) binder. **Table 3** lists the microstructural characteristics, density and Vickers hardness (measured under applying load of 294 N) of the studied material. On the other hand, honing stone chosen as reference was the one tagged as B151/L2/10/50 (B151). It is made from a composite consisting of 12.5 vol% cubic boron nitride (CBN) grains, with size ranging from 126 µm to 150 µm [29,30] (**Figure 4(b)**). The relatively soft coarse-grained cemented carbide was selected as studied material, as its macroscopic mechanical properties are closer to those of the reference honing stone and is expected to exhibit high tolerance to possible damage resulting from localized thermal exposure [31]. Prior to the laser processing, the working surfaces of the samples were mechanically ground and fine polished.

Table 3. Microstructural characteristics, density and hardness of the WC-CoNi cemented carbide grade under consideration.

WC Grain Size (µm)	Co (wt%)	Ni (wt%)	Density (g/cm³)	Hardness (HV30)
Coarse	14	14	12.82	610

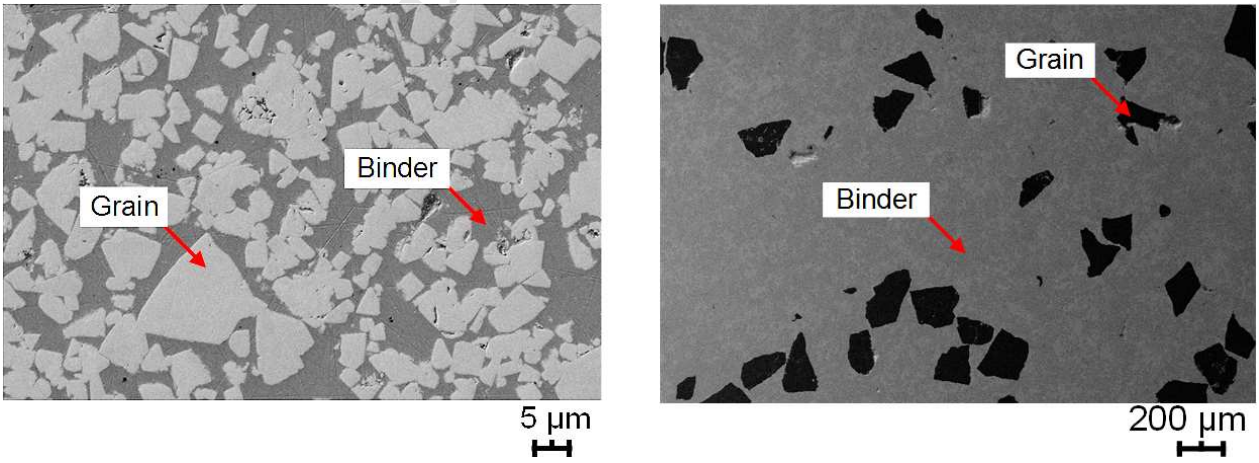

(a) (b)

Figure 4. SEM micrographs showing microstructural aspect of (a) the studied WC-CoNi cemented carbide grade; and (b) CBN honing tool B151 used as reference.

3.2 Reproduction of surface topography on cemented carbide using LST

Ultrafast-laser machining with a picosecond laser system (HYPER25 Coherent Kaiserslautern GmbH) was employed to texture the cemented carbide surface. It was integrated in a 5-axis micromachining system (GL.5, GFH GmbH, **Figure 5(a)**). The high precision machining system can search with a position accuracy of ±1µm and axis speed of 2m/s. Such high precision of the laser beam movement ensures the geometrical accuracy of the produced surface. In the experiments, the used laser beams had a wavelength of 532 nm, pulse duration of 10 ps and fluence of 0.5 J/cm² (**Table 4**). It is reported that more than 75% of the laser beam can be absorbed with a wavelength of 532 nm, and a fluence lower than 2.5 J/cm^2 is suitable to selectively ablate the binder in the nanosecond regime, since the melting and vaporization temperatures of the binder are much lower than those of the WC grains [13]. At the pulse duration of 10 ps, material is removed from the cemented carbide by cold ablation, as a consequence of the short laser-matter reaction time. Nevertheless, some thermal reaction can still be observed at this pulse duration [32,33]. During LST processing, the cemented carbide sample was machined by a laser beam which moved along both x- and y- axis with the speed of 1 m/s, and had a feed speed of 0.2 µm along the z- axis. Hence, in total 130 layers, i.e. 25 µm, were removed by laser beams (**Figure 5(b)**).

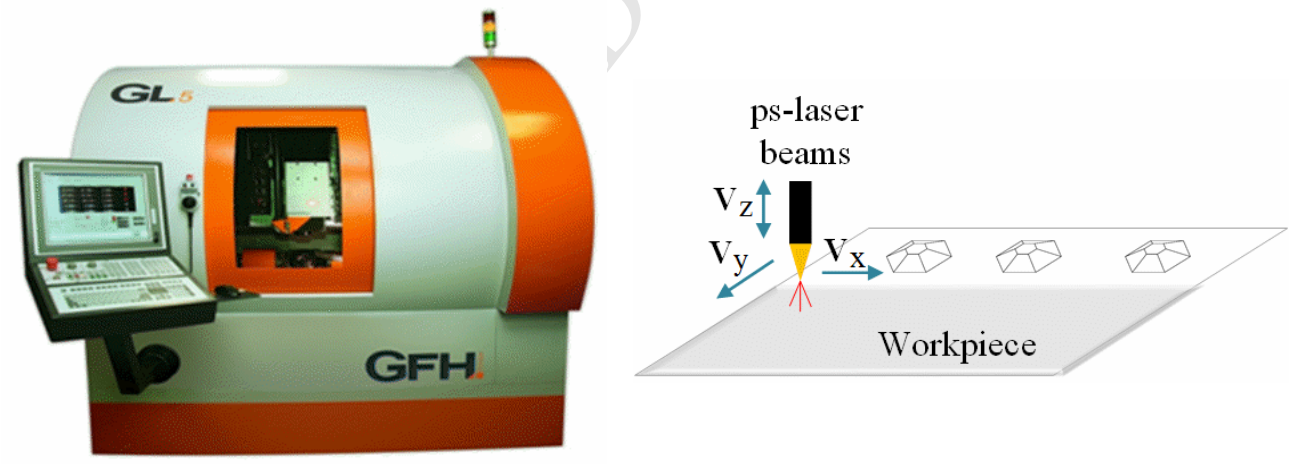

(a) (b)

Figure 5. (a) High precision 5-axis laser micromachining system (GL.5, GFH GmbH). (b) Schematic illustration of surface topography LST manufacturing aimed on the studied cemented carbide.

Table 4. LST configuration and used machining parameters.

Laser type	Laser source	Pulse duration (ps)	Wave length (nm)	Frequency (KHz)	Fluence (J/cm²)

ps-laser	HYPER25	10	532	200	0.5

Once high precision multi-axis laser micromachining system, combined with a picosecond laser, was proven to be suitable for attaining surface topography requirements, surface integrity was assessed. It was done through Field Emission Scanning Electron Microscopy (FESEM) examination, using a JEOL JSM-7001 F unit. Inspection was conducted directly on the laser-processed surface as well as on Focused Ion Beam (FIB) milled cross-sections, within the pyramid body, attained by using a dual beam Workstation (Zeiss Neon 40).

3.3 Cutting capability testing of cemented carbide tool

Aiming to preliminarily evaluate the honing (material removal) capability of the LST processed WC-CoNi cemented carbide, an abrasive machining test was finally conducted. In doing so, an in-house testing workbench, built with the concept of external honing to test the cutting performance of abrasive tools (**Figure 6(a)**), was employed [21]. In this system, the workpiece is fixed on the spindle; thus, it rotates and oscillates at certain speed. Meanwhile, the test tool sample moves towards the workpiece at certain feed speed. Workpiece material is then removed by the sharp cutting edges of the test tool during the rotation, aiming to improve (through a honing-like action) the surface quality of the workpiece.

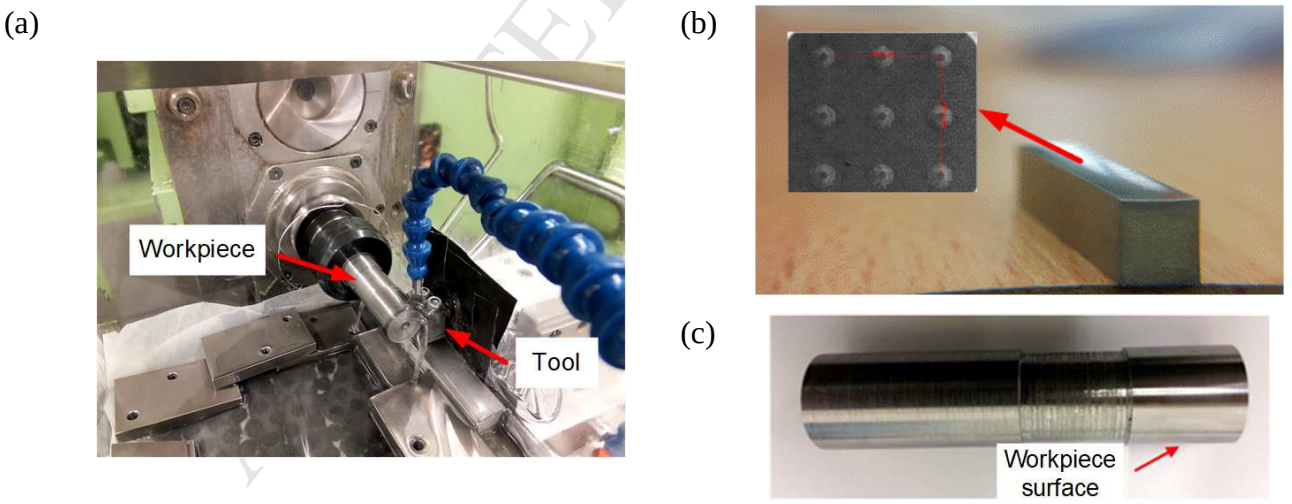

Figure 6. (a) In-house built testing workbench for abrasive machining processes; (b) WC-CoNi cemented carbide tool with LST processed hexagonal pyramid patterns, and (c) counterpart made of steel.

Testing conditions (**Table 5**) include rotation and oscillation of workpiece at speeds of 500 r/min and 1000 mm/min, respectively. The used lubricant Kadio50 had a kinematic viscosity υ of 5 mm^2/s at the

temperature of 40 °C. The flow rate of the lubricant was set to 0.07 Bar. The initial applied normal force on the test tool was about 25 N. The whole test was conducted with lubrication, and lasted about 420 s.

Table 5. Machining parameters and workbench configuration.

Rotation speed (rpm)	Oscillation speed(mm/min)	Oscillation number	Feed(µm)	Flow rate(bar)	Lubricant viscosity (mm²/s)
500	1000	20	2	0.07	5

In this cutting test, the LST processed WC-CoNi cemented carbide was used as test tool sample. The honing stone B151/L2/10/50 (B151) was also tested as the reference sample. The honing stone had been dressed before the test to reveal the cutting edges. Both of the samples had the same dimension of 20×3×4.95 mm. Microstructural aspect (B151) and surface topography features (WC-CoNi) are summarized in **Table 1**. It should be highlighted that sculpted pyramids are uniform in shape and regularly distributed over the surface of WC-CoNi tool. This is different from the conventional honing tool, where CBN grains are distributed randomly, and their shapes can vary from circle to elongated, although most of them exhibit rather either rectangle or hexagonal geometries [34].

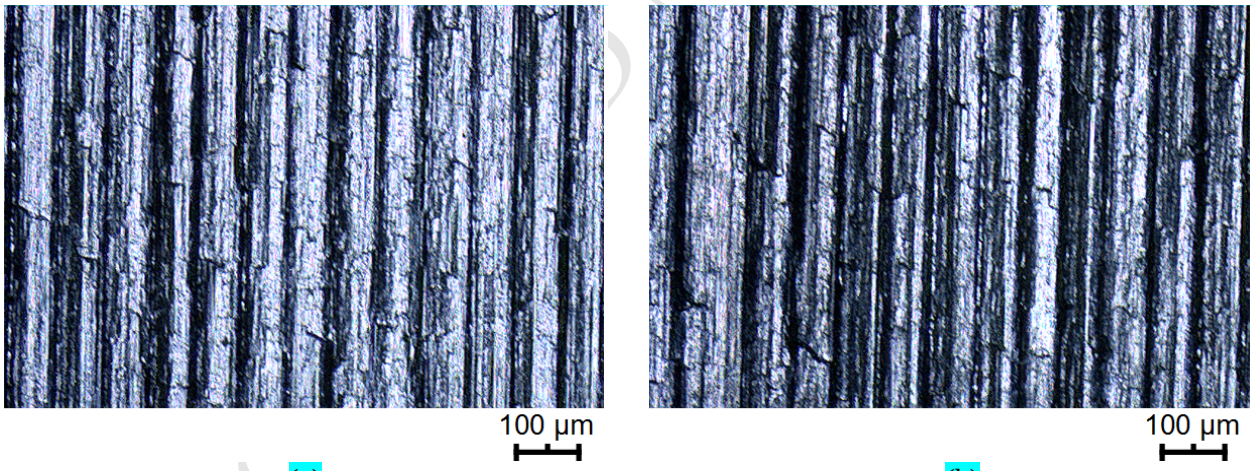

Figure 7. Surface characterization (LSM) and profiles of (a) workpiece 1, (b) workpiece 2.

The counterpart (workpiece) was made of steel 20MnCr5, and its working surface had been fine-turned before the machining test (**Figure 6(c)**). **Figures 7(a) and (b)** show the surface inspection of two workpieces after fine turning. The strips were induced in the turning processes, and some cracks can also be detected. R_a, R_z and R_{max} were selected to describe the surface conditions of the workpieces and measured values are given in **Table 6**. Workpieces 1 and 2 were machined by the B151 honing stone and the hardmetal tool, respectively. Once cutting capability was validated,

surface conditions of the cemented carbide tool were characterized in terms of surface degradation and microstructural changes.

Table 6. Roughness measurements of workpiece 1 and workpiece 2 before testing.

Workpiece	Corresponding tool	Ra (µm)	Rz (µm)	Rmax (µm)
1	B151	3.2	17.7	24.4
2	Hardmetal	3.7	20.1	22.0

4. Results and discussion

4.1 Production of hexagonal pyramids on cemented carbides

4.1.1 Characterization of geometrical properties

Topography reconstructions of the hexagonal pyramids (both array and individual) were done on the basis of data gathered from Laser Scanning Microscopy (LSM) characterization and subsequent analysis using the software Origin 9.0. They are given in **Figures 8(a)** and **(b)** respectively. Scanned surface area is 1024 µm x 1024 µm, and 9 pyramids were measured. Profile coordination was recorded. It is evidenced that laser-processed surface is quite clean. The 9 shaped pyramids are distributed on the surface with almost identical separation distance, and their hexagonal shape may be discerned. The contour lines of the reconstructed models indicate that slopes at each side of the hexagon pyramid are quite smooth. Geometrical characteristics were measured on the basis of the reconstructed models.

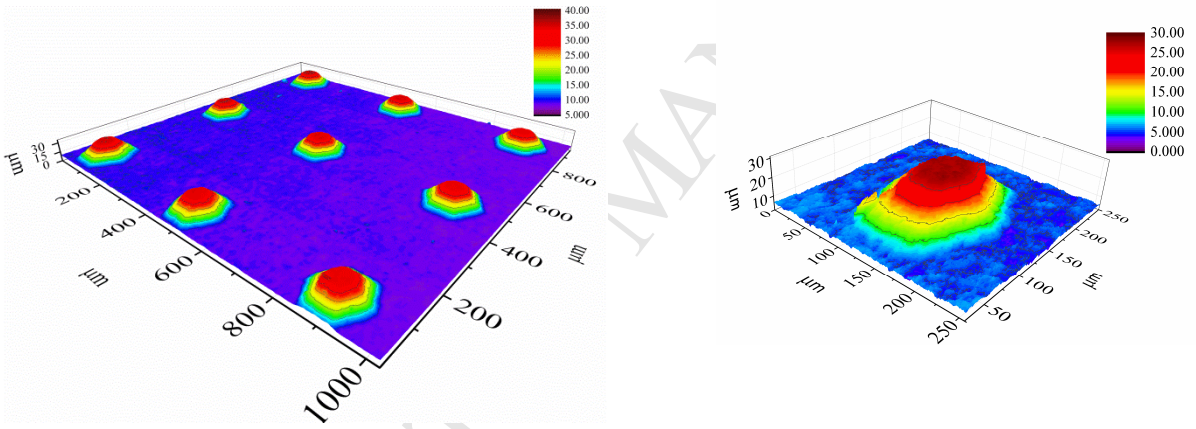

(a) (b)

Figure 8. Surface topography reconstructions (on the basis of LSM data and further analysis using Origin 9.0) of (a) a laser-shaped surface pattern and (b) a single hexagonal pyramid.

Figure 9(a) shows the projection of one single hexagonal pyramid. Three regions may be identified: top, inclined (slope) and bottom. Top (red) and bottom (light blue) are flat, and they are connected by an inclined surface (green). Cross-sectional views at positions A-A and B-B enable to measure slope angles (**Figures 9(b)** and **(c)**).

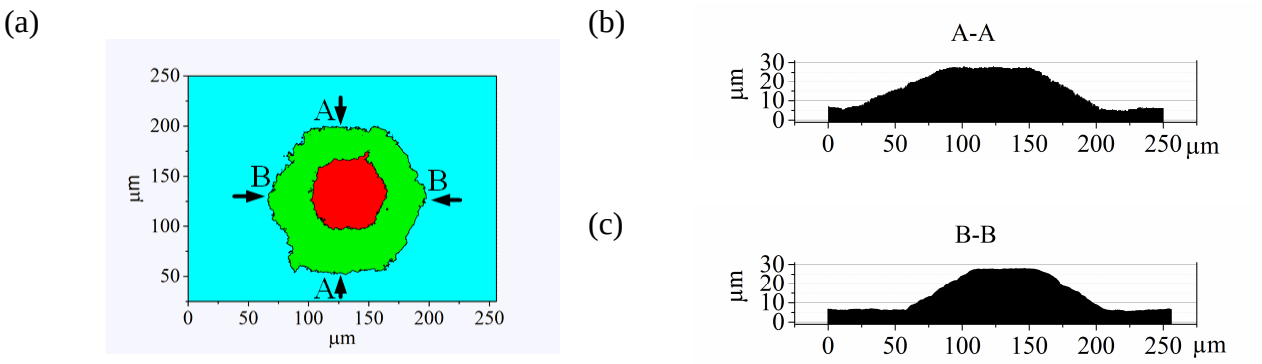

Figure 9. (a) Projection of a single hexagon pyramid, (b) and (c) cross-sectional views at positions A-A and B-B, respectively.

Measurements were carried out and geometrical parameters were determined. **Table 7** summarizes the geometrical characterization of the produced hexagonal pyramid patterns. Hexagonal pyramids exhibited average side lengths a_1 of 60.9 µm and a_2 of 23.5 µm respectively, average height h of 25.7 µm, and areas S_1 of 9.6×10^3 µm^2 at the bottom and S_2 of 1.4×10^3 µm^2 at the top. Finally, average slope angles α (cross section A-A) and β (cross-section B-B) were measured as 31.9º and 35.1° respectively.

Table 7. Geometrical parameters of the LST-shaped hexagonal pyramid patterns.

a_1 (µm)	a_2 (µm)	S_1 ($\times 10^3$µm²)	S_2 ($\times 10^3$µm²)	h (µm)	α (°)	β (°)
60.9	23.5	9.6	1.4	25.7	31.9	35.1

Figure 10 shows the comparison of geometrical properties between aimed and experimentally attained surface topography. In general, a satisfactory agreement is found between attempted and outcome geometrical features. Concordance is generally outstanding regarding pattern geometry. On the other hand, relative differences of the side length a_1 is somehow higher, although still within a small range (15% to 25%). It permits to define agreement as fairly good, when comparing geometry parameters of single hexagonal pyramids. This finding might result from the difficulty of edge determination under the microscopy. This could also apply for explaining relative discrepancies observed in slope values.

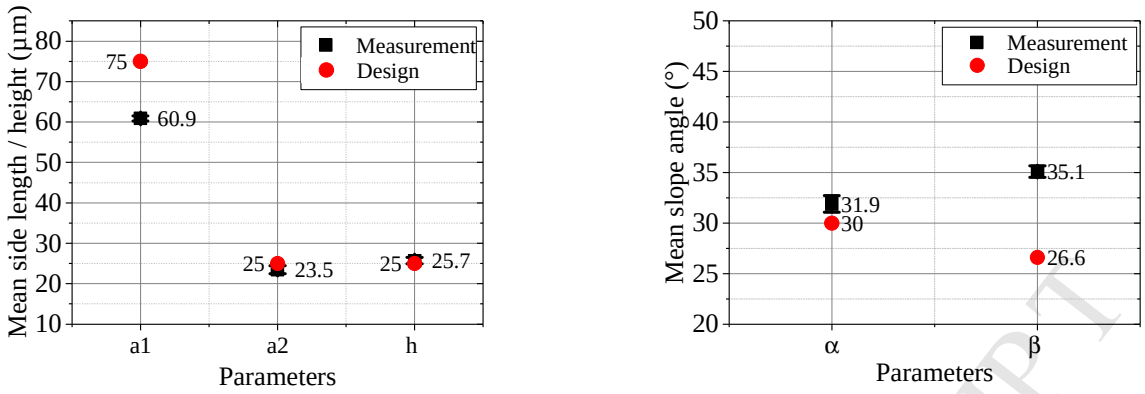

(a) (b)

Figure 10. Comparison of aimed and experimentally attained surface topography features - geometrical parameters of a single hexagonal pyramid: (a) side lengths and height, (b) slope values.

4.1.2. Surface integrity assessment

Figure 11(a) shows the top surface of a LST shaped hexagonal pyramid. Several observations may be highlighted. First, both ceramic and metallic phases are completely and clearly discerned. This is different from the surface aspect attained after shaping of cemented carbides with other conventional non-abrasive machining routes such as EDM (e.g. Ref. [11]). Second, binder is evidenced to experience more pronounced ablation than WC grains. This finding may be rationalized on the basis of the relatively different melting and vaporization temperatures of the two phases (much lower for the CoNi binder) [13,14]. Third, some stripes on the surface of WC grains are evidenced. These stripes are referred to as laser-induced periodic surface structures, and they are produced by the interference of the surface-electromagnetic waves induced by incident laser beams [35-38]. Fourth, coming back to the binder, it is observed that this phase becomes rather blurred due to its melting and incomplete vaporization. This finding indicates that thermal reaction still exists, even under the picosecond mode. However, it is almost negligible when compared to that documented as consequence of rough and/or fine-shaped EDM of cemented carbides (e.g., see Ref. [11]). Such statement is further supported by the FESEM image shown in **Figure 11(b)**, corresponding to a FIB cross-section of one laser-shaped hexagonal pyramid. From this image, it is evident that laser beam action does not affect the subsurface of the laser-treated cemented carbide. Accordingly, neither damage (cracks or pores) nor microstructural changes are discerned within the material bulk, even in regions just below the shaped surface. It points out a negligible influence of LST processing on the surface integrity of patterned cemented carbides.

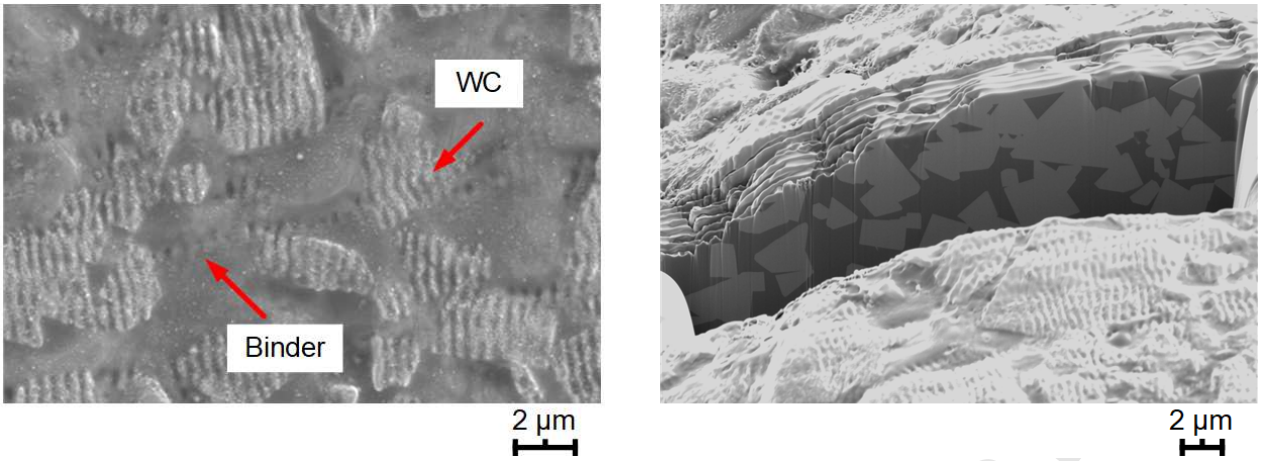

(a) (b)

Figure 11. FESEM images reflecting: (a) surface and (b) subsurface aspect resulting from LST processing of the studied WC-CoNi cemented carbide.

4.2. Validation of cutting capability of LST cemented carbide tool

4.2.1 Improvement of surface finish of the workpiece

Cutting capability of the textured cemented carbide tool was preliminarily evaluated on the basis of surface finish amelioration of the workpieces. As it may be seen in **Figure 12**, strips and cracks induced during previous turning (as-received condition of workpiece, **Figure 7**) were removed during the abrasive test, yielding a final smoother surface finish.

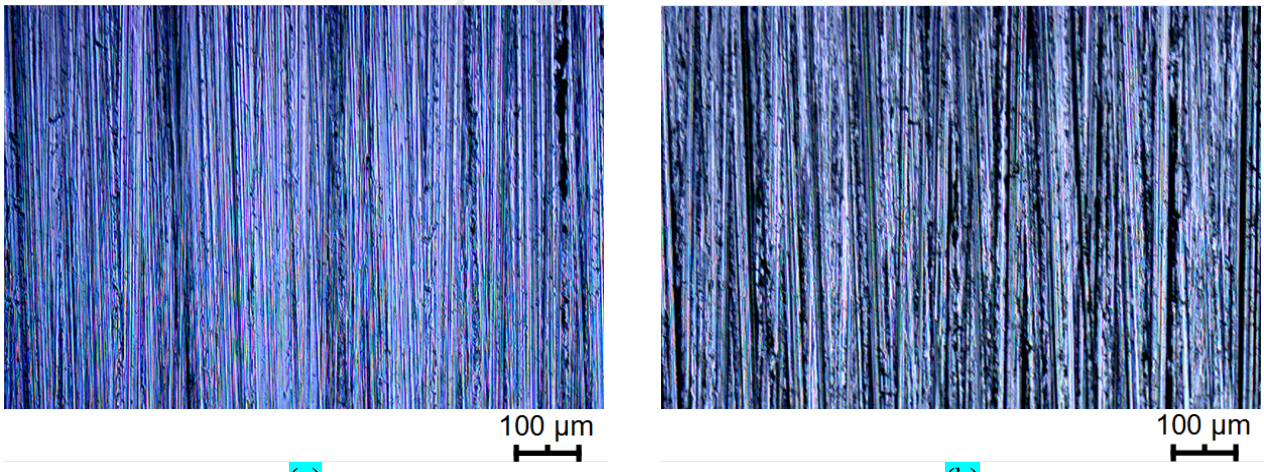

(a) (b)

Figure 12. LSM surface characterization of workpiece after abrasive machining test using: (a) honing stone B151, and (b) LST cemented carbide tool.

Values of roughness attained in the workpiece after abrasive machining test are given in **Figure 13**. It is evident that surface finish of the workpiece has been significantly improved (between 65% and 82% decrease) as a result of the honing-like action done by the surface patterned cemented carbide tool.

Such roughness enhancement is satisfactorily close to relative changes achieved by using the CBN honing stone (range within 75%-90% reduction).

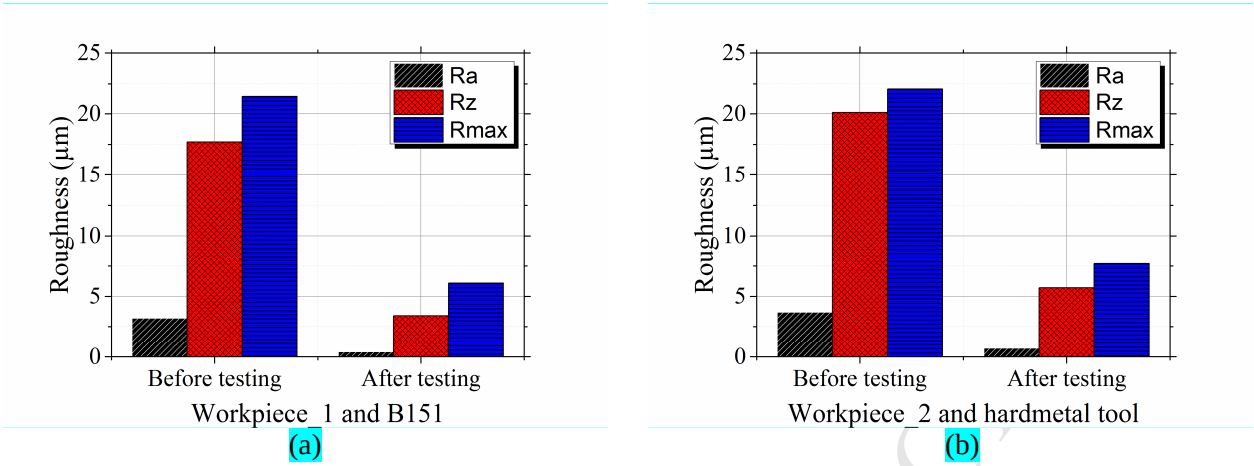

Figure 13. Roughness improvement of the workpiece resulting from abrasive machining test using: (a) honing stone B151, and (b) LST hardmetal tool

4.2.2 Wear characterization of LST cemented carbide tool.

Some geometrical parameters of single laser sculpted pyramids (Table 2) were measured after abrasive machining test. They are compared with values assessed before abrasive testing (**Table 8**). It may be discerned that shape of the sculpted pyramids kept basically unchanged, as illustrated by image reconstructions shown in **Figure 14**. However, pyramid height had obviously diminished (about 4µm). This experimental fact suggests that wear of single pyramids takes place mainly by gradual degradation of the top platform of sculpted geometry. This is completely different from the severe broken up or eruption scenarios, often observed in the honing processes involving CBN or diamond stones.

Table 8. Changes induced in geometry of laser sculpted pyramids of cemented carbide tool, as a result of abrasive machining testing.

Geometry parameter	a_1 (µm)	a_2 (µm)	S1 (x10³ µm²)	S2 (x10³ µm²)	h (µm)	α (°)	β (°)
Before testing	60.9	23.5	9.6	1.4	25.7	31.9	35.1
After testing	59.6	25.9	9.1	2.4	17.7	24.8	27.4

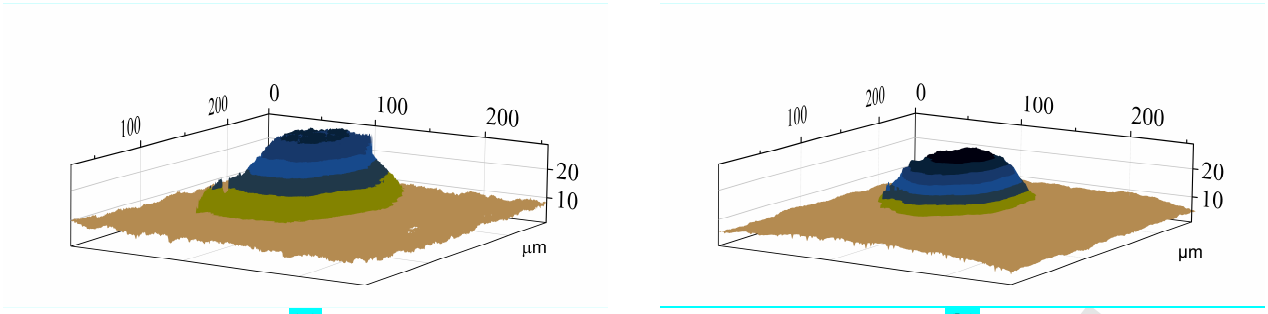

Figure 14. Image reconstruction of geometry of one single hexagonal pyramid: (a) before, and (b)after cutting test.

Surface topography aspect of a representative area of LST hardmetal tool as well as of one single hexagonal pyramid, before and after machining test, are shown in **Figure 15**. As it has been referred above, shape of pyramids was basically unchanged after abrasive action, i.e. hexagonal profile can still be discerned and no obvious disruptive damage has been induced by the cutting process, such as structural collapse, grain eruption or debris stacking, among others. Furthermore, it is also evidenced that surface area surrounding the pyramids experienced negligible damage, since both hardmetal phases, i.e. WC grains and metallic binder, are still discernible. However, and as expected, this is not the case at contacting area and flank, where morphology exhibited relevant changes.

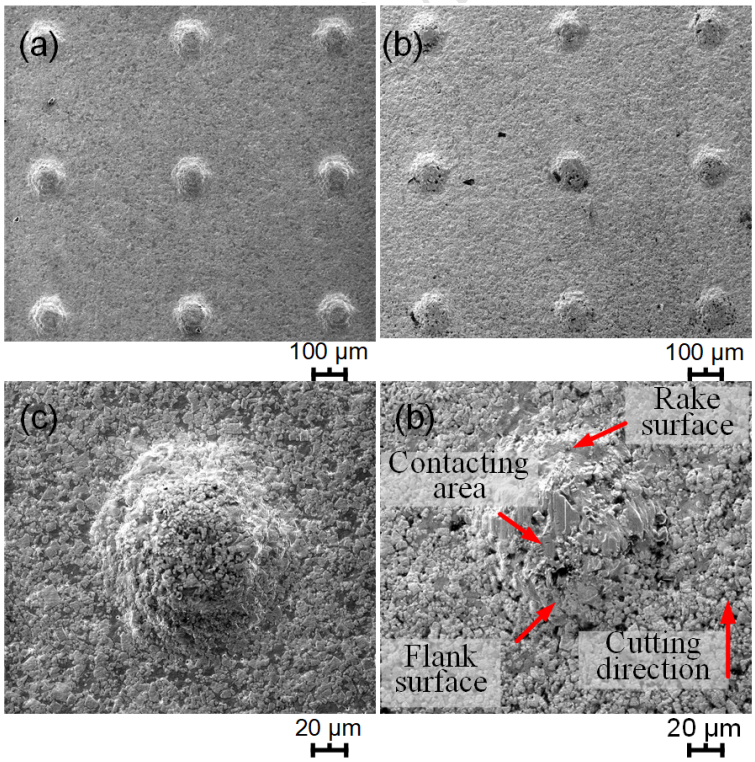

Figure 15. SEM images showing surface topography aspect of LST tool and one single pyramid, before (a and c, respectively), and after (b and d, respectively) abrasive machining test.

Abrasive action resulted in noticeable changes in surface morphology of single pyramids, depending on specific functions and features during the machining process. Contacting area (cutting area) was

the location exposed to pressing and sliding contact, against workpiece, during the penetration of the pyramid (abrasive grain). Hence, it experienced significant and localized pressing and shearing force during the cutting process. As a consequence, sliding traces were observed after the cutting process, as well as evidence of tiny broken grains produced due to pressing (**Figures 16(a) and (d)**). Some micro-cracks were discerned on the sliding traces, possibly resulting from scratches associated with relative sliding against these tiny grains. On the other hand, rake surface (forepart of the cutting edge) had to face direct contact with chips (debris) produced in the cutting process, undertaking then corresponding friction and compression forces. As a result, strips on the grains disappeared and stacking of debris was well pronounced (**Figures 16(b) and (e)**). It should also be highlighted that in borderline between rake surface and contacting area, some cavities were observed. These are speculated to emerge due to the strong impact between the pyramid (abrasive grain) and the counterpart (workpiece). However, surface damage reduced considerably as flank surface is approached and became negligible there, as pointed out by the fact that strips produced by laser are still discernible there (**Figure 16(c) and (f)**).

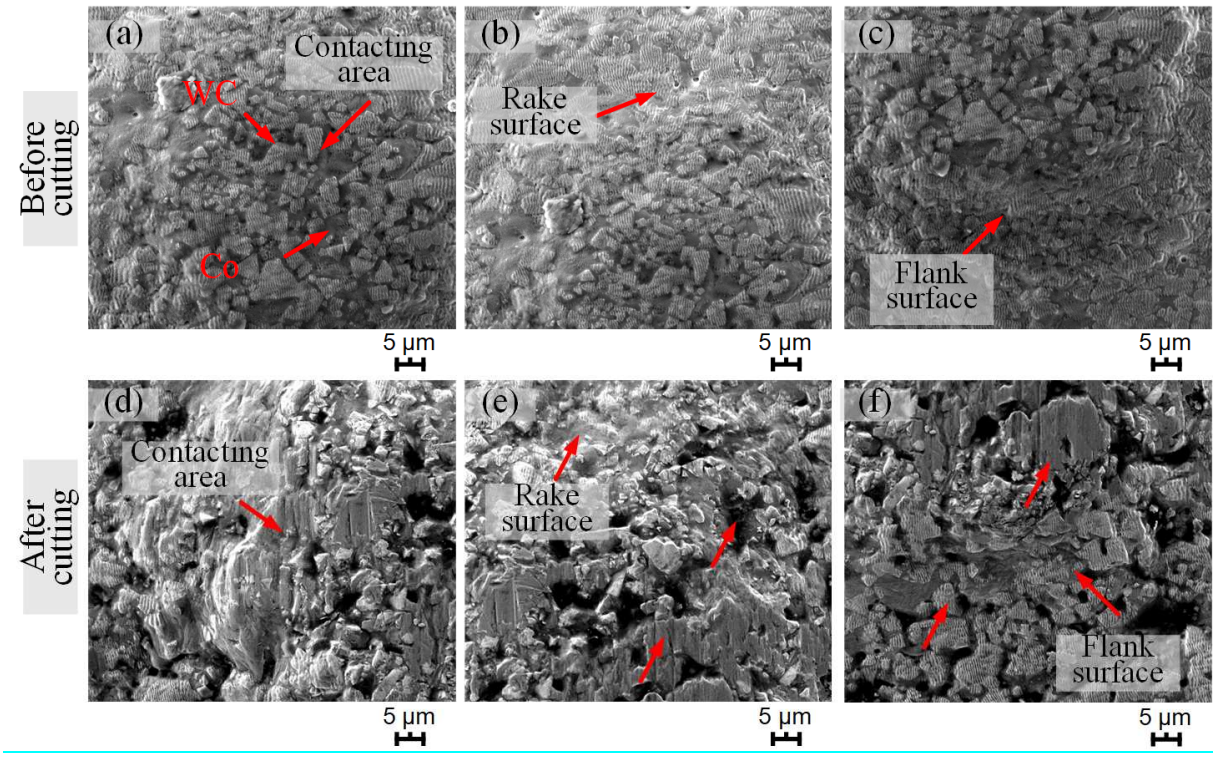

Figure 16. Surface morphological changes within one single pyramid induced by the abrasive machining process: (a) and (d) contacting area, (b) and (e) rake surface, (c) and (f) flank surface.

Finally, the surface morphology analysis was complemented by a subsurface cross-sectional one. It was conducted by FIB milling along cutting direction; hence, it subsequently covered flank surface,

contacting area and rake surface (**Figure 17(a)**). It was found that chips were easily stacked on the rake surface. Corrosion of the binder and micro-cleavage of grains at the subsurface were also found along the whole cutting. However, they were more pronounced on the contacting area and rake surface, where sculpted pyramids suffered more pressure and shearing during the cutting process (**Figure 17(b,c,d)**). Micro-cracks seemed to initiate close to the binder-carbide interfaces, and later penetrated into the grains inducing final cleavage of the hard particles. As the binder was removed, the generated grain micro-debris became free and either flushed away by lubricant action or spread out after chip contact (**Figure 17(e)**).

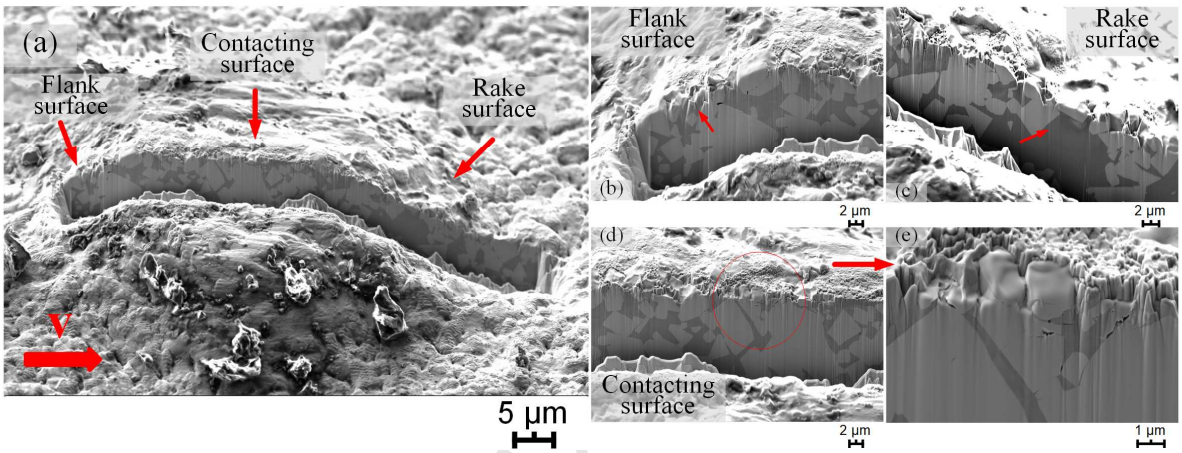

Figure 17. FIB-FESEM cross-sectional analysis of changes induced at the subsurface of one single pyramid as a consequence of the abrasive machining process: (a) overview of the FIB-cutting, (b) flank surface, (c) rake surface, (d) contacting area and (e) higher magnification view of section shown in (d).

5. Concluding remarks

Laser surface texturing of a WC-CoNi cemented carbide grade has been implemented in order to replicate the surface topography of conventional CBN-base honing tools On the basis of the experimental findings, the following conclusions can be drawn:

- Using as reference the surface topography exhibited by traditional CBN honing stones, hexagonal pyramids have been successfully produced by LST as regular patterns on the surface of a WC-CoNi cemented carbide grade. Initial geometrical design of the hexagonal pyramid patterns was aimed for simulating surface topography of CBN honing stone B151.

- A picosecond laser combined with a 5-axis micromachining system was applied to produce the referred surface pattern. A quite satisfactory agreement at micrometer scale was found between aimed and experimentally attained geometrical parameters. Furthermore, direct surface and subsurface inspection by FESEM points out negligible effects of ultra-short laser machining on the surface integrity of the WC-CoNi cemented carbide sample. Hence, LST can be defined as an appropriate approach to simulate the surface topography of honing tools on cemented carbides, with high precision and surface finish quality.

- Preliminary findings from abrasive tests, attempting to simulate honing-like service conditions, demonstrate that LST shaped cemented carbide tools can effectively remove material from a steel workpiece, yielding an enhanced and smoother surface finishing. Within this context, these surface patterned cemented carbide tools emerge then as potential alternative to conventional CBN honing stones. Further research in this area, focused on quantitative analysis of the cutting capability and wear resistance of surface textured cemented carbide tools, is then recalled.

- From the wear characterization of the LST hardmetal tool itself, it is found that it experiences similar degradation micro-mechanisms as those well known for cemented carbides under abrasive conditions, i.e. carbide grains are broken up into tiny pieces and binder is removed by abrasion or adhesion of resulting debris. Regarding wear mode, it should be highlighted that it is different from the one observed for conventional honing tools, under the consideration of a dynamic cutting process. From this viewpoint, the surface topography of the cutting surface of CBN composites maintains a dynamic stability due to the self-dressing phenomena, i.e. new

abrasive grains will come out from the composite matrix when the old ones are worn out. On the other hand, sculpted pyramids in the hardmetal tool exists only on the cutting surface but not in the matrix. In this regard, intrinsic wear resistance of pyramids becomes critical for defining the life of the LST hardmetal tool investigated in this study. Accordingly, performance enhancement must consider microstructural design optimization of the hardmetal grade used for shaping the LST tool aimed for honing-like operation.

Acknowledgements

The work leading to this publication was supported by the German Academic Exchange Service (DAAD) with funds from the German Federal Ministry of Education and Research (BMBF) and the People Program (Marie Curie Actions) of the European Union's Seventh Framework Program (FP7/2007-2013) under REA grant agreement n° 605728 (P.R.I.M.E. – Postdoctoral Researchers International Mobility Experience). The authors would like to express their gratitude to Photonik-Zentrum e.V., Kaiserslautern for supplying equipment support, as well as to KADIA Produktion GmbH + Co. and Saar-Hartmetall und Werkzeuge GmbH for supplying the studied materials. Finally, this contribution has also been partly funded by the Spanish Ministry of Economy and Competitiveness through Grant MAT2015-70780-C4-3P (MINECO/FEDER).

References

[1] Burkhard G, Rehsteiner F, Schumacher B. High efficiency abrasive tool for honing. CIRP Annals - Manufacturing Technology 2002;51:271–4. doi:10.1016/S0007-8506(07)61515-7.

[2] Prakash L. Fundamentals and general applications of hardmetals. In Sarin, VK, Mari D, Llanes L (Eds.), Comprehensive Hard Materials, vol. 1, 2014, p. 29–90. doi:10.1016/B978-0-08-096527-7.00002-7.

[3] Geiger M, Popp U, Engel U. Excimer laser micro texturing of cold forging tool surfaces - Influence on tool life. CIRP Annals - Manufacturing Technology 2002;51:231–4. doi:10.1016/S0007-8506(07)61506-6.

[4] Jacobson S, Hogmark S. Surface modifications in tribological contacts. Wear 2009;266:370–8. doi:10.1016/j.wear.2008.04.035.

[5] Pettersson U, Jacobson S. Influence of surface texture on boundary lubricated sliding contacts. Tribology International 2003;36:857–64. doi:10.1016/S0301-679X(03)00104-X.

[6] Zhang K, Deng J, Xing Y, Li S, Gao H. Effect of microscale texture on cutting performance of WC/Co-based TiAlN coated tools under different lubrication conditions. Applied Surface Science 2015;326:107–18. doi:10.1016/j.apsusc.2014.11.059.

[7] Ibatan T, Uddin MS, Chowdhury MAK. Recent development on surface texturing in enhancing tribological performance of bearing sliders. Surface and Coatings Technology 2015;272:102–20. doi:10.1016/j.surfcoat.2015.04.017.

[8] Mezghani S, Demirci I, Zahouani H, Mansori M El. The effect of groove texture patterns on piston-ring pack friction. Precision Engineering 2012;36:210–7. doi:10.1016/j.precisioneng.2011.09.008.

[9] Etsion I. State of the art in laser surface texturing. Journal of Tribology 2005;127:248. doi:10.1115/1.1828070.

[10] Ta VD, Dunn A, Wasley TJ, Li J, Kay RW, Stringer J, et al. Laser textured surface gradients. Applied Surface Science 2016;371:583–9. doi:10.1016/j.apsusc.2016.03.054.

[11] Llanes L, Martinez E, Idañez E, Casas B, Esteve J. Influence of electrical discharge machining on the sliding contact response of cemented carbides. International Journal of Refractory Metals and Hard Materials 2001;19:35–40.

[12] Jahan MP, Rahman M, Wong YS. A review on the conventional and micro-electro discharge machining of tungsten carbide. International Journal of Machine Tools and Manufacture 2011;51:837–58. doi:10.1016/j.ijmachtools.2011.08.016.

[13] Li T, Lou Q, Dong J, Wei Y, Liu J. Selective removal of cobalt binder in surface ablation of tungsten carbide hardmetal with pulsed UV laser. Surface and Coatings Technology 2001;145:16–23. doi:10.1016/S0257-8972(01)01288-9.

[14] Dumitru G, Romano V, Weber HP, Sentis M, Marine W. Ablation of carbide materials with femtosecond pulses. Applied Surface Science 2003;205:80–5. doi: 10.1016/S0169-4332(02)00906-6.

[15] Dumitru G, Lüscher B, Krack M, Bruneau S, Hermann J, Gerbig Y. Laser processing of hardmetals: Physical basics and applications. International Journal of Refractory Metals and Hard Materials 2005;23:278–86. doi:10.1016/j.ijrmhm.2005.04.020.

[16] Karatas C, Yilbas BS, Aleem A, Ahsan M. Laser treatment of cemented carbide cutting tool. Journal of Materials Processing Technology 2007;183:234–40. doi:10.1016/j.jmatprotec.2006.10.012.

[17] Wang HP, Guan YC, Zheng HY. Smooth polishing of femtosecond laser induced craters on cemented carbide by ultrasonic vibration method. Applied Surface Science 2017;426:399–405. doi:10.1016/j.apsusc.2017.07.160.

[18] Konrad W, Claus D, Marcel H, Christian W. Laser prepared cutting tools. Physics Procedia 2012;39:240–8. doi:10.1016/j.phpro.2012.10.035.

[19] Breidenstein B, Denkena B, Bergmann B, Krödel A. Laser material removal on cutting tools from different materials and its effect on wear behavior. Met Powder Rep 2016;0:1–6. doi:10.1016/j.mprp.2016.06.001.

[20] Bouzakis KD, Charalampous P, Kotsanis T, Skordaris G, Bouzakis E, Denkena B, et al. Effect of HM substrates' cutting edge roundness manufactured by laser machining and micro-blasting on the coated tools' cutting performance. CIRP Journal of Manufacturing Science and Technology 2017;18:188–97. doi:10.1016/j.cirpj.2017.02.003.

[21] Fang S, Herrmann T, Rosenkranz A, Gachot C, Marro FG, Mücklich F, et al. Tribological performance of laser patterned cemented tungsten carbide parts. Procedia CIRP 2016;42:439–43. doi:10.1016/j.procir.2016.02.228.

[22] Aurich JC, Herzenstiel P, Sudermann H, Magg T. High-performance dry grinding using a grinding wheel with a defined grain pattern. CIRP Annals - Manufacturing Technology 2008;57:357–62. doi:10.1016/j.cirp.2008.03.093.

[23] Deng H, Chen GY, Zhou C, Li SC, Zhang MJ. Processing parameter optimization for the laser dressing of bronze-bonded diamond wheels. Applied Surface Science 2014;290:475–81. doi:10.1016/j.apsusc.2013.11.120.

[24] Li HN, Axinte D. Textured grinding wheels: A review. International Journal of Machine Tools and Manufacture 2016;109:8–35. doi:10.1016/j.ijmachtools.2016.07.001.

[25] Flores G. Grundlagen und Anwendungen des Honens [Fundamentals and Applications of Honing]. Vulkan-Verlag; 1992: 60-63.

[26] Fang S, Llanes L, Engstler M, Baehre D, Soldera F, Muecklich F. Surface topography quantification of super hard abrasive tools by laser scanning microscopy. Materials Performance and Characterization 2016;5:20160008. doi:10.1520/MPC20160008.

[27] Ding W, Linke B, Zhu Y, Li Z, Fu Y, Su H, et al. Review on monolayer CBN super abrasive wheels for grinding metallic materials. Chinese Journal of Aeronautics 2017;30:109–34. doi:10.1016/j.cja.2016.07.003.

[28] Ichida Y, Sato R, Kajino H. Development of Ultrafine-Crystalline cBN Abrasive Grains for Innovative Grinding Technology. In: Mitsuishi M, Ueda K, Kimura F, editors. Manufacturing Systems and Technologies for the New Frontier: The 41st CIRP Conference on Manufacturing Systems May 26--28, 2008, Tokyo, Japan, London: Springer London; 2008, p. 463–6. doi:10.1007/978-1-84800-267-8_95.

[29] FEPA standard, Shapes and dimension for diamond & CBN grinding wheels, Federation of European Producers of Abrasives, Paris, France, 1992:64.

[30] Klocke F. Manufacturing Processes 2. Grinding, Honing, Lapping. vol. 53. 2013. doi:10.1017/CBO9781107415324.004.

[31] Tarragó JM, Dorvlo S, Esteve J, Llanes L. Influence of the microstructure on the thermal shock behavior of cemented carbides. Ceramics International 2016;42:12701–8. doi:10.1016/j.ceramint.2016.05.024.

[32] Yao YL, Chen H, Zhang W. Time scale effects in laser material removal: a review. The International Journal of Advanced Manufacturing Technology 2005;26:598–608. doi:10.1007/s00170-003-2026-y.

[33] Chichkov BN, Momma C, Nolte S, von Alvensleben F, Tünnermann A. Femtosecond, picosecond and nanosecond laser ablation of solids. Applied Physics A: Materials Science & Processing 1996;63:109–15. doi:10.1007/s003390050359.

[34] Fang S, Llanes L, Bähre D, Mücklich F. 3D characterization of cubic boron nitride (CBN) composites used as tool material for high precision abrasive machining processes. Ceramics International 2017;43:14693–700. doi:10.1016/j.ceramint.2017.07.198.

[35] Bonse J, Rosenfeld A, Krüger J. On the role of surface plasmon polaritons in the formation of laser-induced periodic surface structures upon irradiation of silicon by femtosecond-laser pulses. Journal of Applied Physics 2009;106:104910. doi:10.1063/1.3261734.

[36] Okamuro K, Hashida M, Miyasaka Y, Ikuta Y, Tokita S, Sakabe S. Laser fluence dependence of periodic grating structures formed on metal surfaces under femtosecond laser pulse irradiation.

Physical Review B - Condensed Matter and Materials Physics 2010;82:1–5. doi:10.1103/PhysRevB.82.165417.

[37] Bonse J, Krüger J, Höhm S, Rosenfeld A. Femtosecond laser-induced periodic surface structures. Journal of Laser Applications 2012;24:42006. doi:10.2351/1.4712658.

[38] Shukla P, Waugh DG, Lawrence J, Vilar R. Laser surface structuring of ceramics, metals and polymers for biomedical applications. Laser Surface Modification of Biomaterials, Elsevier; 2016, p. 281–99. doi:10.1016/B978-0-08-100883-6.00010-1.

Highlights

- Pyramids similar to CBN grains were sculpted on WC-CoNi cemented carbide surfaces.
- Surface topography of the CBN honing stone has been reproduced on the surface of cemented carbide.
- High geometric precision is achieved using ultra-short pulse laser.
- Surface integrity does not get affected by the laser processing.
- Similar cutting ability to regular honing stone has been achieved by the patterned cemented carbide.